Synchronization and desynchronization under the influence of quasiperiodic forcing

Eireen Neumann,[1] Irina Sushko,[2] Yuri Maistrenko,[2] and Ulrike Feudel[3]
[1]*Department of Physics, University of Potsdam, Am Neuen Palais, PF 601553, D-14415 Potsdam, Germany*
[2]*Institute of Mathematics, Academy of Sciences of Ukraine, 3 Tereshchenkivska Street, Kiev 252601, Ukraine*
[3]*Institute for Chemistry and Biology of the Marine Environment, University of Oldenburg, PF 2503, D-26111 Oldenburg, Germany*
(Received 26 July 2002; published 5 February 2003)

We study the influence of quasiperiodic forcing on synchronization and desynchronization using two coupled quasiperiodically forced logistic maps as a paradigm. We show that due to the forcing the synchronization region in parameter space shrinks. The loss of transverse stability of the synchronized attractors leads to desynchronization. Two types of such blowout bifurcations are described, namely, the blowout bifurcations of synchronized quasiperiodic motion on invariant curves and synchronized strange nonchaotic attractors, both yielding desynchronized chaotic attractors.

DOI: 10.1103/PhysRevE.67.026202 PACS number(s): 05.45.Xt, 05.45.Ac

I. INTRODUCTION

Synchronization phenomena of coupled chaotic systems as well as mechanisms leading to desynchronization have attracted much interest in the last decade of the second millenium. Considering interacting identical chaotic oscillators, different synchronization phenomena can be observed in dependence on the coupling strength: We speak about phase synchronization [1] if the oscillators adjust their phases such that the mean frequencies of the chaotic oscillations coincide, whereas their amplitudes vary chaotically in time. For increased coupling strength one can achieve a complete synchronization [2]. In this case, not only the phases but also the amplitudes develop in precisely the same way. The motion of the two coupled systems takes place in an invariant subspace of the state space. The concept of complete synchronization has been generalized by releasing the requirements of the actual equality of the variables of the coupled systems. Instead, in general synchronization, the dynamical variables of both subsystems obey a certain functional dependency [3,4]. Not only the types of synchronization were of interest, but also the mechanisms leading to the loss of chaotic synchronization. Assuming the existence of a completely synchronized chaotic attractor, then different invariant sets in the invariant subspace can become transversally unstable in the transition to a desynchronized state: First, particular unstable periodic orbits embedded in the synchronized chaotic attractor lose their transverse stability giving rise to the emergence of riddled basins (riddling bifurcation [5,7]). Second, the whole attractor in the invariant subspace loses its transverse stability in average leading to a blowout bifurcation [6,7].

In this paper we study the influence of quasiperiodic driving on synchronization and the different transitions to a nonsynchronized state. As a first approach it has been shown that synchronization can appear in quasiperiodically forced systems in Ref. [8]. We use two quasiperiodically forced coupled logistic maps as a paradigm. The general dynamics of two coupled logistic maps without forcing has been extensively investigated [9–11]. In Ref. [12] this system has been considered as an application to interdependent open economics. Our main focus is the study of the changes in the bifurcation phenomena due to the influence of a quasiperiodic driving force.

In quasiperiodically forced systems a special type of attractors, namely, strange nonchaotic attractors (SNAs) present a characteristic dynamical behavior in between regularity and chaos. This type of dynamics has been first described by Grebogi *et al.* [13] and can be defined as a closed invariant attractive set which is not piecewise differentiable and for which the typical orbits have nonpositive Lyapunov exponents. Thus, SNAs have a fractal structure like usual strange attractors, but there does not exist any sensitivity with respect to changes in the initial conditions: no exponential divergence of trajectories can be observed. The property of nondifferentiability has been used in Ref. [14] to construct a method for distinguishing between SNAs and regular attractors in quasiperiodically forced systems. This method relies on the sensitivity of SNAs with respect to the phase of the external force and is used here to identify SNAs. (To be more specific: In contrast to regular attractors, the derivative with respect to the phase of the external driving grows unboundedly in the case of SNA. In the present paper the strangeness of nonchaotic attractors is detected via the criterion of phase sensitivity.) The emergence of SNAs can be expected in the synchronized state as well as in the nonsynchronized one.

The coexistence of synchronized and nonsynchronized attractors in some regions of parameter space is important for establishing the type of transition to a nonsynchronized state. The transition occurs via a blowout bifurcation when the synchronized attractor loses its transverse stability. The coexistence of two SNAs, synchronized and nonsynchronized has been demonstrated recently, for a small range of parameters in the system of two coupled quasiperiodically forced logistic maps [15]. In contrast to our present investigations, a nonlinear coupling and a nonsymmetric quasiperiodic external forcing has been applied in Ref. [15].

Due to the presence of quasiperiodic forcing we obtain changes in the dynamical behavior and in the types of transitions to a nonsynchronized state. The dynamics of coupled quasiperiodically forced maps is very rich: quasiperiodic behavior with two and three incommensurate frequencies, phase locking phenomena, strange nonchaotic and chaotic

attractors can be found. Moreover, the dynamics can take place on an invariant subspace, the diagonal plane $D=\{(x,y,\theta):x=y\}$, x and y denote the states of the two subsystems, respectively, and θ is the phase of the external driving. In this invariant subspace the motion of both coupled maps is fully synchronized. We focus on this synchronized behavior and discuss the possible mechanisms for the loss of synchronization when the synchronized state becomes transversally unstable. We show, in particular, which transitions from synchronized to nonsynchronized behavior can be observed in the case of *nonchaotic* attractors in D.

The outline of the paper is the following. In Sec. II we introduce the model and investigate the influence of the strength of quasiperiodic driving on the size and the shape of the synchronization region in parameter space and on bifurcations taking place for synchronized attractors. Then, in Sec. III we study, in more detail, which types of attractors can occur in the synchronization region and use the phase sensitivity method [14] for distinguishing between regular motion and SNAs. We find that the synchronized motion can coexist with the nonsynchronized one. Parameter regions of multistability are obtained in Sec. IV. The bifurcations of the synchronized attractors under quasiperiodic forcing leading to a loss of synchronization are described in Sec. V. We discuss several types of blowout bifurcations whose characteristics will be analyzed in Sec. VI. In particular, we demonstrate two types of this bifurcation, namely, transitions from synchronized quasiperiodic motion and synchronized SNA to nonsynchronized chaotic attractors. Finally, we summarize our findings in Sec. VII.

II. MODEL

We consider a system of two coupled logistic maps which are externally forced,

$$\begin{aligned} x_{n+1} &= \alpha x_n(1-x_n)+\beta(y_n-x_n)+\epsilon\cos(2\pi\theta_n),\\ y_{n+1} &= \alpha y_n(1-y_n)+\beta(x_n-y_n)+\epsilon\cos(2\pi\theta_n),\\ \theta_{n+1} &= \theta_n+\omega(\mathrm{mod}\,1), \end{aligned} \tag{1}$$

where the parameter α is the strength of nonlinearity, β is the coupling strength, ϵ and ω are amplitude and frequency of the external driving force, respectively. Throughout the paper the frequency ω is chosen to be equal to the inverse of the golden mean $\omega=(\sqrt{5}-1)/2$, i.e., the driving is quasiperiodic.

In general, the dynamics takes place in the three-dimensional phase space (x,y,θ). Stable synchronized dynamics can be observed in an invariant two-dimensional subspace $D=\{(x,y,\theta):x=y\}$. Such synchronous motion can be found in some region of parameters α, β, and ϵ. Thus, the synchronized attractor lives on the diagonal plane D, and the dynamics on it is governed by the single logistic map with quasiperiodic forcing

$$\begin{aligned} x_{n+1} &= \alpha x_n(1-x_n)+\epsilon\cos(2\pi\theta_n),\\ \theta_{n+1} &= \theta_n+\omega(\mathrm{mod}\ \ 1). \end{aligned} \tag{2}$$

For zero amplitude of the quasiperiodic driving, $\epsilon=0$, the two equations of Eq. (2) become uncoupled. We obtain the well-known logistic map $x_{n+1}=\alpha x_n(1-x_n)$ which displays a period-doubling cascade to chaos as the bifurcation parameter α increases. Thus, for $\epsilon=0$ the synchronized dynamics is either regular (periodic) or chaotic. As soon as the driving is switched on ($\epsilon>0$), the periodic orbits P_k of the logistic maps are transformed into invariant curves mapped into each other cyclically with the period k. We will denote them by kIC. We would like to note that in invertible maps the same types of transitions are expected to occur though their study is a bit more complicated. In this case the invariant curves in invertible maps can be considered as Poincaré sections of tori in flows in contrast to the invariant curves observed in noninvertible maps. But in the literature [16,17] often the term torus is used for an invariant curve also in noninvertible maps. To avoid confusion, we use the terms ''torus'' and ''torus doubling'' in the following only if we refer to articles where these terms are used.

The dynamics of the quasiperiodically forced logistic map has been investigated from different points of view in Refs. [16,17]. Heagy and Hammel [16] have described notable effects of the quasiperiodic driving, e.g., bifurcation points of torus doubling are shifted to larger values of α, the threshold for chaos is lowered and the torus-doubling cascade is truncated. Kuznetsov *et al.* [17] investigate in detail the terminal point of torus doubling depending on the forcing amplitude. We will show that the effects of quasiperiodic forcing in the system of two coupled logistic maps are similar to those of a single map under the influence of an external quasiperiodic forcing. Moreover, beside quasiperiodic and chaotic motion we find the existence of strange nonchaotic attractors (SNA) as a characteristic type of synchronized dynamics caused by quasiperiodic driving.

For system (1), we determined the regions in the (α,β)-parameter plane where synchronized dynamics can occur for different values of the external forcing amplitude ϵ. To this end, the transverse Lyapunov exponent is calculated as

$$\lambda_\perp=\lim_{N\to\infty}\frac{1}{N}\sum_{n=1}^{N}\ln|f'_\alpha(x_n)-2\beta|, \tag{3}$$

where f'_α denotes the derivative of the logistic function $f_\alpha(x)=\alpha x(1-x)$ with respect to x. Negative values of $\lambda_\perp$ characterize the region in parameter space where the synchronized attractor is at least weakly stable or stable in Milnor sense [18]. In the case of a synchronized chaotic attractor $A^{(s)}$ weak stability means that $A^{(s)}$ is transversally stable in average, i.e. almost all trajectories on $A^{(s)}$ are transversally stable. For a nonchaotic attractor on D, weak stability coincides with Lyapunov stability.

To characterize the inner dynamics of the synchronized attractor, the longitudinal Lyapunov exponent

$$\lambda_\parallel=\lim_{N\to\infty}\frac{1}{N}\sum_{n=1}^{N}\ln|f'_\alpha(x_n)| \tag{4}$$

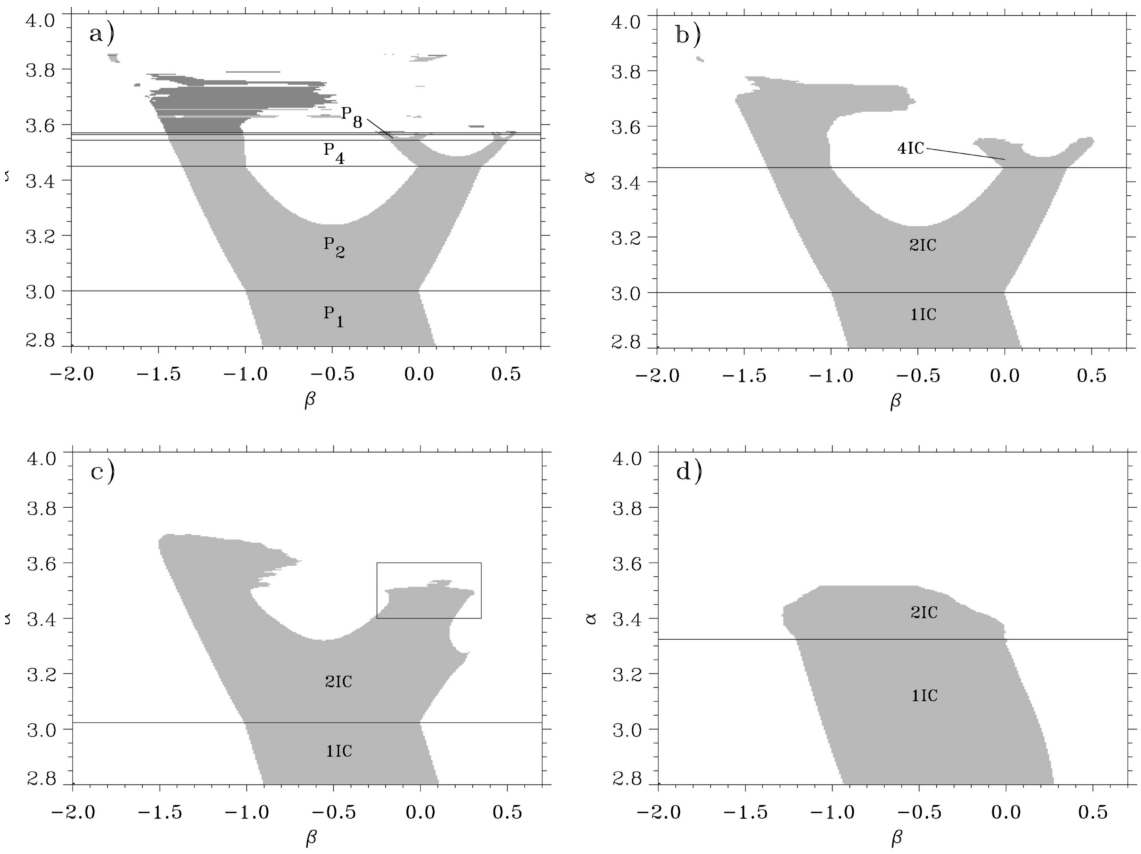

FIG. 1. The region of synchronized motion in the (α,β)-parameter plane (chaos–dark gray) for (a) $\epsilon=0$ (periodic orbits—light gray), (b) $\epsilon=0.003$ (invariant curves—light gray), (c) $\epsilon=0.03$, and (d) $\epsilon=0.1$. The little box of panel (c) is shown enlarged in Fig. 2

has to be calculated. It measures the strength of exponential divergence of trajectories along the diagonal. The synchronized attractor is chaotic if the longitudinal Lyapunov exponent is positive. With the variation of a system parameter the synchronized attractor loses its transverse stability leading to nonsynchronized behavior. This bifurcation, called blowout bifurcation, occurs when $\lambda_\perp$ becomes positive.

Afterwards, the synchronized invariant set is a repeller, i.e., typical trajectories will be repelled from it and will approach some other attractor in phase space or will diverge to infinity. Blowout bifurcations are detectable by monitoring the transverse Lyapunov exponent when the system parameter is varied: $\lambda_\perp$ changes its sign from negative to positive at the moment of blowout bifurcation. The stable dynamical regime after the bifurcation can be characterized by the two Lyapunov exponents of the new born asynchronous attractor $A^{(a)}$. If the larger of both Lyapunov exponents is positive ($\lambda_{\max}>0$) then $A^{(a)}$ is a chaotic attractor.

To illustrate the effects of external quasiperiodic driving on system (1), we restrict ourselves on four values of the driving amplitude ϵ. Figures 1(a), 1(b), 1(c) and 1(d) show the region in the (α,β)-parameter plane where the synchronized attractor is weakly stable for driving amplitudes $\epsilon=0$, $\epsilon=0.003$, $\epsilon=0.03$, and $\epsilon=0.1$, respectively. This synchronization region has a treelike structure, whose size slowly decreases, and small branches are cutoff with increasing external driving force ϵ. In the unforced case $\epsilon=0$, the synchronized attractor [gray region in Fig. 1(a)] is either a periodic orbit (light gray region) or a chaotic attractor (dark gray region). The period-doubling cascade is infinite and the lines of the doubling bifurcation are parallel to the β axis at values of α where the period doublings in the logistic map take place. The synchronization region has a complicated internal structure and includes islands which correspond to the periodic windows of the map f_α.

For $\epsilon>0$ the synchronized periodic orbits are transformed into smooth invariant curves of corresponding periodicity. We observe doubling bifurcations of invariant curves instead of period-doubling bifurcations of periodic orbits. Figures 1(b), 1(c), and 1(d) demonstrate that the doublings of invariant curves are delayed with $\epsilon>0$, i.e., they occur at larger values of α. As it is known [17], the doubling cascade of tori (in our example: invariant curves) is truncated. This truncation corresponds to a successive cutoff of the branches of the tree-like synchronization region. Depending on the amplitude of quasiperiodic driving ϵ, branches of the tree are cutoff, first those corresponding to the stability region of invariant curves with higher periodicity. The transition to chaos via SNA can be observed just inside the region of weak stability. Note also that even at small forcing strength $\epsilon=0.003$ most islands of weak stability, separated from the main bifurcation tree, vanish. Moreover, due to the cutoff of the branches of the synchronization tree, the synchronization region shrinks in size. As a consequence it becomes more and more difficult

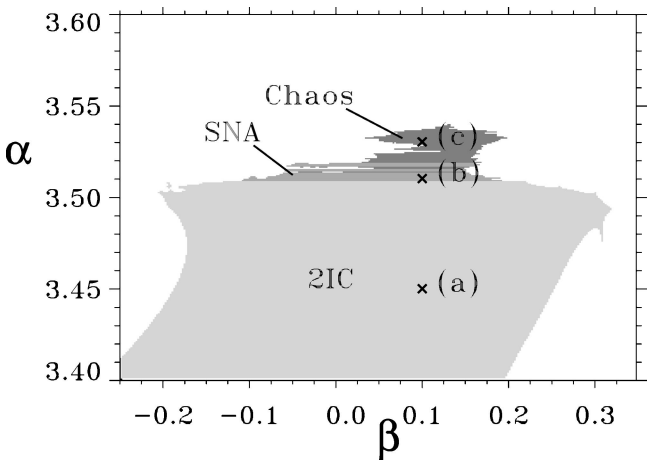

FIG. 2. Enlarged box from Fig. 1(c), different gray scale denotes different dynamical behavior, two invariant curves 2IC (light gray), SNA (gray), and chaos (dark gray). The crosses mark the positions for which the representants of the different dynamical behavior have been calculated (see Fig. 3).

to obtain synchronized motion when the forcing is increased. For $\epsilon=0.1$ the synchronization region ends already at $\alpha \approx 3.5$ [Fig. 1(d)], and for $\epsilon=0.3$ synchronization cannot be found at all. Thus, the synchronized motion is suppressed for a sufficiently high amplitude of quasiperiodic forcing.

III. SYNCHRONIZED DYNAMICS

There are different types of synchronized dynamics, i.e., dynamics on the diagonal plane. It is governed by system (2), and hence does not depend on the coupling parameter β. Which type of synchronized attractor occurs, depends, if ϵ is fixed, on the value of nonlinearity parameter α only. Lines of doubling bifurcations of smooth invariant curves are parallel to the β axis (see Fig. 1).

To discuss the attractor types in detail we choose a fixed driving amplitude ϵ, say $\epsilon=0.03$. The doubling cascade of invariant curves is truncated just before the second doubling. We find in the synchronization region either 1 or 2 invariant curves (1IC or 2IC), or SNAs or chaotic behavior. Figure 2 shows a blowup of the little box in Fig. 1(c) which includes transitions from quasiperiodicity (light gray) via SNA (gray) to chaotic behavior (dark gray). The regions of different dynamical regimes have been estimated by computing the longitudinal Lyapunov exponent, which is positive for chaotic attractors but negative for SNA and quasiperiodic motion. To distinguish between the latter two attractors, both with negative Lyapunov exponent, one has to analyze the sensitivity of the attractor with respect to phase variation of the external force. The method to apply (suggested in Ref. [14]) is based on the property of SNA to be a nonsmooth (fractal) invariant set which is not piecewise differentiable (see the definition of an SNA given in Ref. [13]). It consists of an attempt to calculate the derivative with respect to the external phase. This derivative is bound in the case of a smooth attractor, while in the case of SNA, the calculated values of the derivative cannot be bound, since this derivative in fact does not exist. SNA and invariant curves have been distinguished numerically using this property.

To illustrate the dynamical regimes of system (1), we present attractors calculated at three parameter points marked by crosses in Fig. 2. Figures 3(a), 3(b), and 3(c) show characteristic examples of the different types of synchronized dynamics, i.e., smooth invariant curves, SNA, and chaotic attractor, for three values of the nonlinearity parameter $\alpha_1=3.45$, $\alpha_2=3.51$, $\alpha_3=3.53$, and coupling parameter $\beta=0.1$.

These attractors are (at least) weakly stable, i.e., the transverse Lyapunov exponent is less than zero. The invariant curves [Fig. 3(a)] and the SNA [Fig. 3(b)] have also negative longitudinal Lyapunov exponent while for the chaotic attractor [Fig. 3(c)] it is positive.

The mechanisms leading to strange nonchaotic behavior in the system of two coupled quasiperiodically driven logistic maps are the same as for the single logistic map under quasiperiodic driving, because the synchronized dynamics takes place in the two-dimensional subspace $(x=y,\theta)$. The transition from two-frequency quasiperiodic motion (on 2 invariant curves 2IC) to SNA has been found to be related to the truncated torus-doubling cascade: A collision of the stable doubled-curve 2IC with its unstable parent 1IC has been found for the parameter values shown in Fig. 3. With increasing parameter α, the two invariant curves 2IC [Fig. 3(a)] become more wrinkled and come closer to the unstable invariant curves 1IC from which they were formerly born by

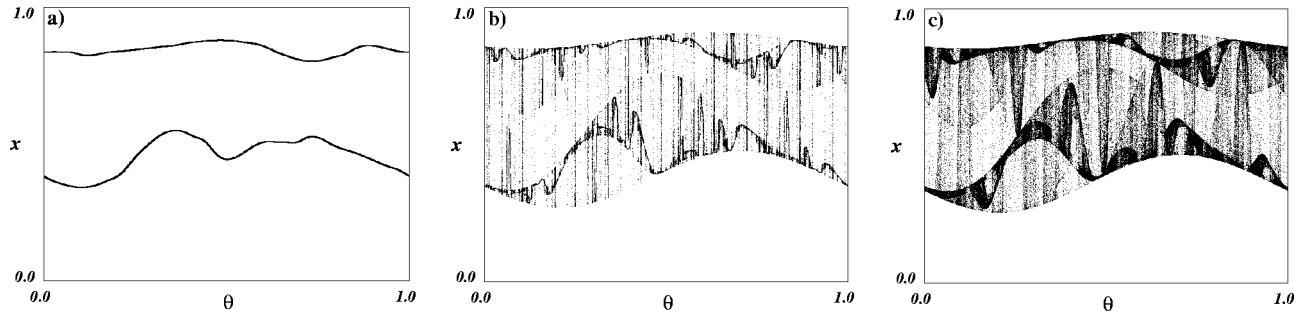

FIG. 3. Representants of the dynamics in the region of synchronized dynamics. The panels correspond to the points marked by crosses in the bifurcation diagram in Fig. 2 at $\beta=0.1, \epsilon=0.03$, and at different values of α. Panel (a) shows two invariant curves representing a period-two attractor at $\alpha=3.45$, panel (b) represents a strange nonchaotic attractor at $\alpha=3.51$, and panel (c) represents a chaotic attractor at $\alpha=3.53$ as possible types of synchronized motion.

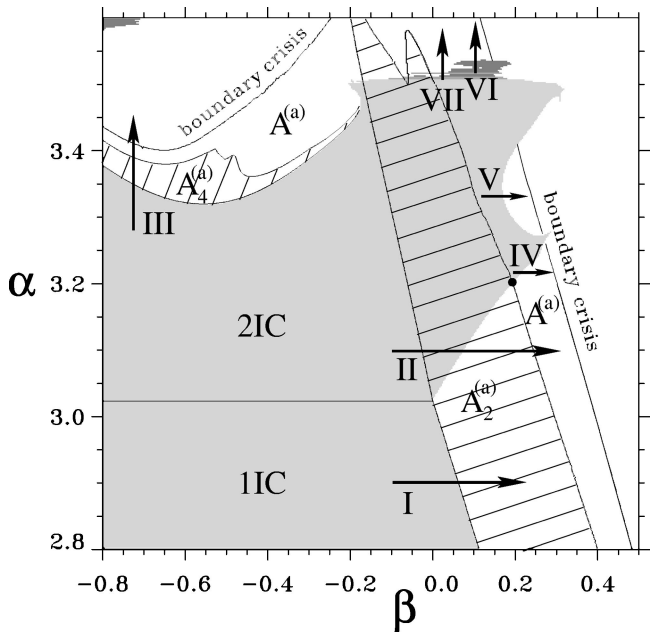

FIG. 4. The region of weak stability of synchronized attractors (coded in same gray scale as in Fig. 2) in the (α,β)-parameter plane for $\epsilon=0.03$ and bifurcation lines of the asynchronous attractors.

a doubling bifurcation. At the bifurcation point they finally collide with the unstable parent in a dense set of θ values but not in all values of θ. As a result, an SNA is observed [Fig. 3(b)]. Further increasing of the bifurcation parameter α leads to a chaotic attractor [Fig. 3(c)]. Finally, when α is so large that $\lambda_\perp$ becomes positive, the chaotic attractor in the diagonal plane loses its transverse stability and the trajectory either approaches another attractor outside the diagonal plane (discussed in Sec. V) or diverges to infinity.

It should be mentioned that in general for systems whose undriven counterparts exhibit a period-doubling cascade to chaos also other mechanisms of transition to SNA are possible as the fractalization route to SNA by Nishikawa and Kaneko [19], and the intermittency route to SNAs by Prasad *et al.* [20].

IV. COEXISTENCE OF SYNCHRONOUS AND ASYNCHRONOUS MOTION

The coexistence of an attractor outside the diagonal with the synchronized attractor plays a crucial role for the type of transitions in the moment of a loss of transverse stability. Therefore, we should first analyze whether there exist attractors out of the diagonal in an appropriate parameter range which contains the curve of synchronization loss. The corresponding nonsynchronous dynamical behavior might be a quasiperiodic motion on invariant curves as well as chaotic or strange nonchaotic behavior.

The gray region in Fig. 4 shows the region of weak stability of the synchronized attractor in the (α,β) parameter plane for $\epsilon=0.03$. The horizontal black line at $\alpha_c \approx 3.023425$ denotes the first doubling of invariant curves $(1\mathrm{IC}\rightarrow 2\mathrm{IC})$ in the invariant subspace D.

The borderline of the gray bifurcation tree corresponds to the transverse instability of the synchronized attractor. Passing this curve by varying the parameters α and/or β, the dynamics in the diagonal plane D becomes transversally unstable (the transverse Lyapunov exponent $\lambda_\perp$ becomes positive). As a result, either a new asynchronous attractor containing the formerly transversally stable synchronized solution appears (blowout bifurcation) or the trajectory can approach another, asynchronous attractor or diverge to infinity. The region $A_2^{(a)}$ in Fig. 4 is the region of the existence of an asynchronous two-piece attractor outside the diagonal plane. Thus, the intersection of the synchronization region of two invariant curves (2IC) (gray) with the region $A_2^{(a)}$ is a region of bistability. Depending on the initial condition either the synchronous or the asynchronous attractor can be obtained.

For $\alpha<\alpha_c\approx 3.023\,425$ the left border of the region $A_2^{(a)}$ coincides with the line corresponding to the loss of the transverse stability of the synchronized invariant curve 1IC. Here, a supercritical transverse doubling takes place. The invariant curve 1IC loses its transverse stability giving rise to the emergence of an asynchronous two-piece attractor, consisting of two invariant curves. They map one into another, representing a period-two attractor. Such type of synchronization loss takes place when the border of the bifurcation tree is passed along path I in Fig. 4 .

As already mentioned, for larger values of α, the transverse instablity curve intersects the existence region $A_2^{(a)}$ of the nonsynchronized two-piece attractor. Let us cross the border of the bifurcation tree with $\alpha=3.1$ fixed, and β varied along path II in Fig. 4. To the left of region $A_2^{(a)}$ the synchronized invariant curve 1IC, already being unstable along the diagonal, becomes additionally transversally unstable, giving rise to an asynchronous attractor consisting of two invariant curves. emerged by a subcritical bifurcation from 1IC. After this bifurcation the two invariant curves are not stable, but they stabilize at the left border of $A_2^{(a)}$. Moreover, the loss of transverse stability of 1IC leads to the emergence of a repelling tongue that develops from 1IC. Due to the quasiperiodic driving, a dense set of tongues (with respect to θ) appears, and the trajectory is transversally repelled from the synchronized invariant curve. Therefore, after entering the region of bistability (intersection of regions 2IC and $A_2^{(a)}$), it depends on the initial conditions which attractor is approached by the trajectory, the two-frequency quasiperiodic motion on two invariant curves either in the diagonal plane D or outside D. Figure 5(a) shows the projection of both possible types of attractors onto the (x,y) plane, as well as their basins of attraction to vizualize the repelling tongue, for parameter values $\alpha=3.1$, $\beta=0.06$, and fixed driving amplitude $\epsilon=0.03$.

At the parameter value $\alpha=3.1$ along path II the transverse instability curve lies inside the region $A_2^{(a)}$. Varying β beyond the border of the gray region (region of transverse stability of two invariant curves 2IC) all observed trajectories start to approach the existing asynchronous attractor. The synchronized two invariant curves have lost their transverse stability in a subcritical transverse doubling bifurcation when

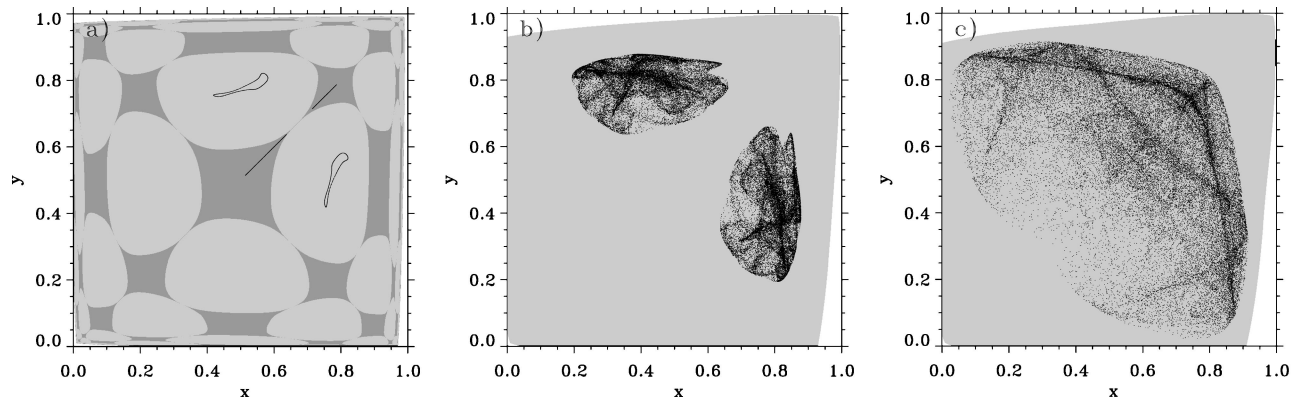

FIG. 5. Projection of attractors onto the (x,y) plane at parameters $\epsilon=0.03$, $\alpha=3.1$, and at different values of β: (a) for $\beta=0.06$ quasiperiodic motion on two invariant curves either synchronized (basin is dark gray) or nonsynchronized (basin is light gray), (b) for $\beta=0.22$ asynchronous two-piece chaotic attractor, and (c) for $\beta=0.3$ asynchronous one-piece chaotic attractor arising after the merging of the formerly two-piece attractor. In all examples, the basin of the attractor at infinity is left blank.

passing the border of the bifurcation tree. For the asynchronous attractor we find that it undergoes a number of bifurcations as β increases towards the right border of region $A_2^{(a)}$ to become an asynchronous two-piece chaotic attractor. Figure 5(b) shows the chaotic attractor, obtained for $\beta=0.22$ and $\alpha=3.1$. It grows in size with increasing β and finally the two pieces merge when β reaches the right border of $A_2^{(a)}$. Beyond the right border of $A_2^{(a)}$ we observe an asynchronous one-piece chaotic attractor including the diagonal plane D. Attractors of this type exist in the parameter region $A^{(a)}$ which is shown in Fig. 4, too. See Fig. 5(c) for an example of an asynchronous chaotic attractor including the diagonal plane at parameter values $\beta=0.3$ and $\alpha=3.1$. The asynchronous attracting set continues to grow in size as β increases until it finally touches its basin boundary (boundary crisis line). After the boundary crisis, the asynchronous attractor disappears, and the trajectory diverges to infinity.

When following path II after having entered the region $A_2^{(a)}$, we pass two different bifurcation lines meeting at a vertex point $(\alpha,\beta)\approx(3.2,0.2)$ in the parameter plane marked by a fat black dot in Fig. 4. Let us discuss this vertex point in more detail. A schematic representation of this vertex including all the different bifurcation lines that meet there is shown in Fig. 6. We have to distinguish two different scenarios when changing β with α fixed above or below the vertex point, respectively. Below the vertex point, for $\alpha<3.2$, we cross first the border of the gray synchronization region being the line of transverse instability of the synchronous attractor in the diagonal. After this crossing the synchronous attractor is unstable and all trajectories are attracted by the asynchronous attractor out of the diagonal, which consists of two pieces. At the second bifurcation line these two pieces merge and a one-piece asynchronous attractor is formed.

Above the vertex, for $\alpha>3.2$, we cross first the right border of the dashed region $A_2^{(a)}$ inside the gray synchronization region (Fig. 4) limiting the region of bistability. At this line the asynchronous attractor out of the diagonal undergoes a basin boundary crisis and disappears. To illustrate this boundary crisis, which is different from the boundary crisis beyond which trajectories go to infinity, we present Fig. 7 which shows the coexisting synchronized and asynchronous attractors and their basins of attraction for a certain θ section $(\theta=0)$ shortly before the boundary crisis of the asynchronous attractor at parameter values $\alpha=3.22$ and $\beta=0.182$. To the right of the region of bistability only the synchronized attractor 2IC is stable inside the synchronization region (gray region in Fig. 4). The second bifurcation line crossed with increasing β above the vertex corresponds to the border of the synchronization region. Here, a blowout bifurcation of the synchronized attractor can be observed. This bifurcation leads to an asynchronous attractor which includes the diagonal and is considered in Sec. V in more detail.

The dashed region $A_4^{(a)}$ in Fig. 4 marks the region in (α,β)-parameter plane where the asynchronous four-piece attractors exist. This type of attractor does not coexist with synchronized attractors; since the region $A_4^{(a)}$ does not intersect the gray bifurcation tree. The lower border of $A_4^{(a)}$ coincides with the transverse instability curve of the bifurcation tree. Passing the curve (for example, along path III in Fig. 4), the synchronized two invariant curves become transversally unstable in a supercritical transverse doubling bifurcation yielding an asynchronous attractor consisting of four invariant curves. As α increases the attractor undergoes some bi-

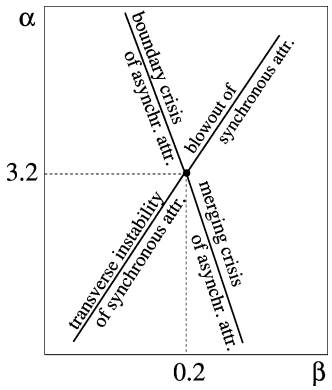

FIG. 6. Schematic representation of the four different types of bifurcation lines meeting at the parameter point $(\alpha,\beta)\approx(3.2,0.2)$ marked as a fat black dot in Fig. 4.

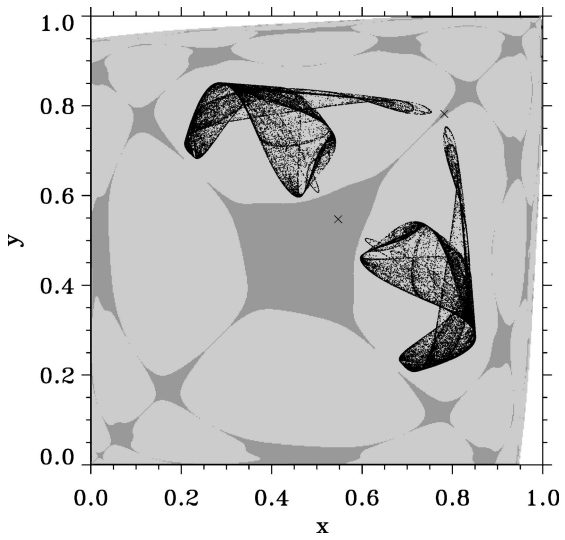

FIG. 7. The asynchronous chaotic attractor out of the diagonal and its basin of attraction in light gray ($\epsilon=0.03$, $\alpha=3.22$, and $\beta=0.182$) shortly before its boundary crisis. The two crosses mark the position of the synchronized two invariant curves and their basin is shown in dark gray. Both attractors (the synchronous and the asynchronous one) present a period-two attractor. The attractors as well as their basin of attraction are presented for the θ section $\theta=0$.

furcations to become an asynchronous four-piece chaotic attractor. The latter one merges to an asynchronous two-piece chaotic attractor including a part of the diagonal plane D when entering the region $A^{(a)}$. The resulting attractor grows in size as α increases and finally touches its basin boundary and disappears (boundary crisis). Thus, it is the same topological situation as has been discussed above for the region $A_2^{(a)}$.

V. BLOWOUT TRANSITIONS

We have demonstrated in the preceding section, that synchronized attractors can coexist with asynchronous ones in an appropriate region of the (α,β)-parameter plane (Fig. 4). As already mentioned, the characteristics of bifurcations from synchronized to nonsynchronized behavior changes at the vertex point considered in Sec. IV. Above the vertex point $(\alpha,\beta)\approx(3.2,0.2)$, we find a blowout transition leading to a new asynchronous attractor which includes the diagonal plane D or some part of D. Let us discuss first the blowout transitions from synchronized two invariant curves to a nonsynchronized chaotic motion, corresponding to the transitions along paths IV and V in Fig. 4.

Along path IV we observe a blowout bifurcation which corresponds to a direct transition from synchronized quasiperiodic motion to nonsynchronized chaotic motion (see Fig. 8). This is to the best of our knowledge a type of blowout bifurcation which has not been observed in unforced cases. First, the transverse Lyapunov exponent $\lambda_\perp$ is less than zero as well as the longitudinal Lyapunov exponent $\lambda_\parallel$ [Fig. 8(e)]. Passing the border of the synchronization region with increasing β (which corresponds to entering the region $A^{(a)}$ along path IV), the transverse Lyapunov exponent $\lambda_\perp$ changes its sign. Accordingly, the synchronized two invariant curves become transversally unstable, and we observe a blowout transition to a nonsynchronized attractor. The maximal Lyapunov exponent $\lambda_{\max}$ after the transition is positive, hence the asynchronous attractor is a chaotic one. The asynchronous chaotic attractor grows in size as β increases and vanishes again in a boundary crisis.

For larger values of α we observe a blowout bifurcation with different features. This type of transition sketched by path V in Fig. 4 may yield to either an asynchronous chaotic attractor or an asynchronous SNA. Let us first consider the case of blowout transition to an asynchronous chaotic attractor (Fig. 9). The longitudinal Lyapunov exponent $\lambda_\parallel$ is less than zero and does not change its value since it does not depend on the varied bifurcation parameter β. It only depends on α which is kept constant along path V in Fig. 4. Therefore, $\lambda_\parallel$ is omitted in Fig. 9(e). At $\beta\approx0.1715$, $\lambda_\perp$ changes its sign from negative to positive. Then, the synchronized two invariant curves become transversally unstable. The maximal Lyapunov exponent $\lambda_{\max}$, coinciding with the transversal one before the blowout transition, is positive but small in a narrow parameter range of β beyond the blowout bifurcation curve. The asynchronous chaotic attractor [Figs. 9(c) and 9(d)] still represents an attractor of period two, including a part of the diagonal plane D. The size of this attracting set emerging in a supercritical blowout bifurcation from quasiperiodic motion on 2IC is small. It is restricted to a narrow region near the formerly synchronized solution. With increasing β, we observe a relatively sudden growth in the magnitude of the maximal Lyapunov exponent $\lambda_{\max}$ which corresponds to a second bifurcation. Beyond this bifurcation the asynchronous chaotic attractor increases quickly in size. Additionally, it consists now only of one piece including the diagonal plane D [Figs. 9(e) and 9(f)]. This bifurcation looks like an interior crisislike phenomenon, but seems to have some different properties as explained below. A further increase of β leads to a further growth of the attractor size until the boundary crisis is reached. After the boundary crisis all observed trajectories diverge to infinity.

For slightly different values of α, the previously described blowout transition (close to path V in Fig. 4) can be also of another type. The blowout transition to an asynchronous attractor can go via SNA, as illustrated by Figs. 10(a)–10(e). By increasing β we observe again a blowout transition, the transverse Lyapunov $\lambda_\perp$ exponent becomes positive. The maximal Lyapunov exponent coincides with the transverse one before the blowout bifurcation. After the bifurcation, $\lambda_{\max}$ becomes negative again in a narrow interval of β. The attractor after the transition has a strange geometrical structure, representing a period-two SNA including a part of the diagonal plane D. It is restricted to a very narrow region around D. Note, that the magnitude of Lyapunov exponents is in the order of 10^{-3}. Moreover, the structure of the SNA is comparable to that of the chaotic attractor considered above. This transition from synchronous quasiperiodic motion to asynchronous SNA resembles the one described in Ref. [21] where the transition to SNA in some other map has been

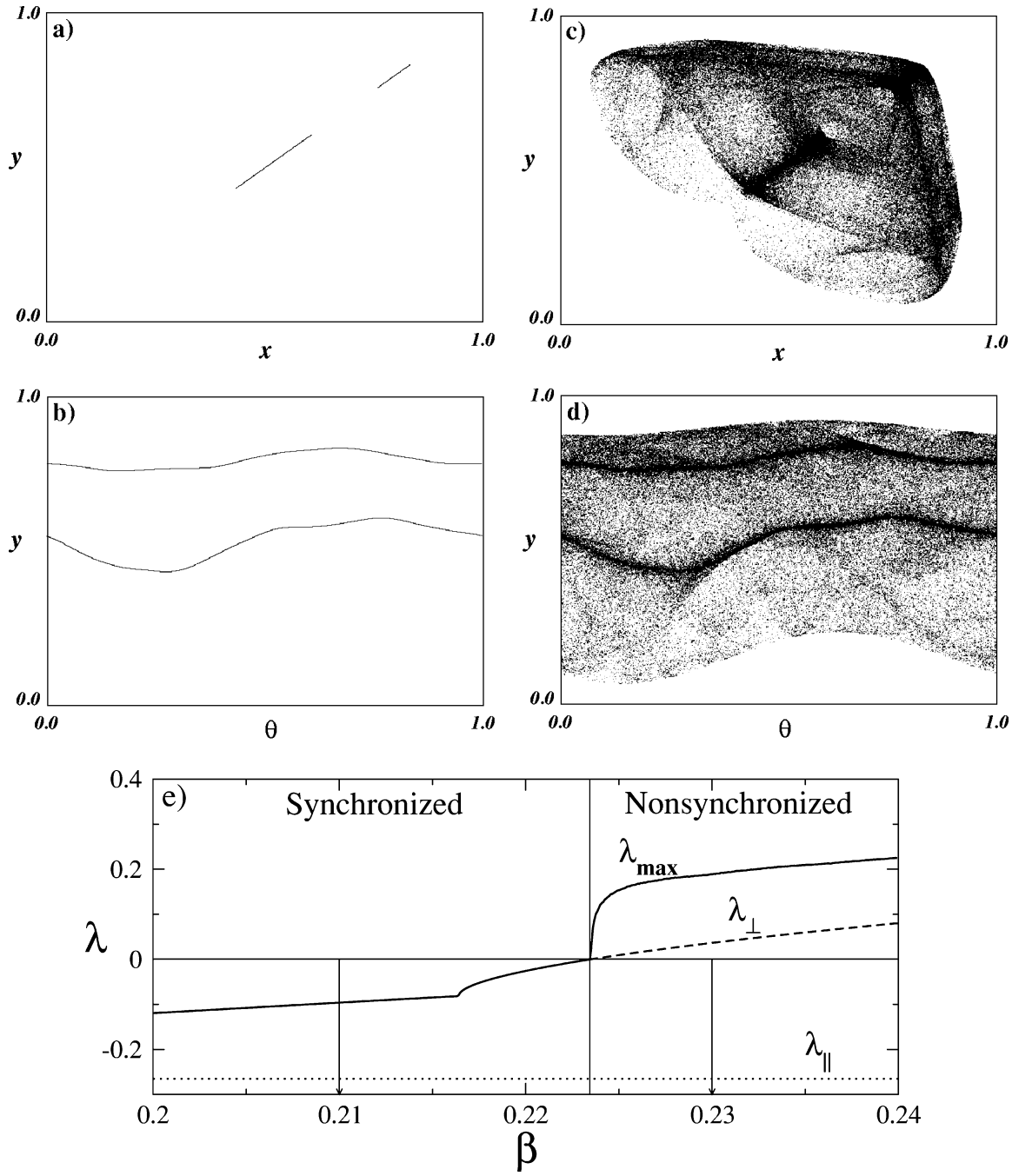

FIG. 8. Blowout transition from two synchronized invariant curves to nonsynchronized chaotic attractor at $\epsilon=0.03, \alpha=3.22$ represented by path IV in Fig. 4. Panels (a) and (b) show the synchronized two invariant curves at $\beta=0.21$ as projection onto the (x,y) plane and onto the y-θ plane, respectively. Panels (c) and (d) show the nonsynchronized chaotic attractor at $\beta=0.23$ as projection onto the x-y plane and onto the y-θ plane after the blowout transition. Panel (e) shows the dependence of Lyapunov exponents $\lambda_\perp$ (dashed), $\lambda_\parallel$ (dotted), and $\lambda_{\max}$ (solid) on the bifurcation parameter. The arrows mark the values of the bifurcation parameter β for which the attractors have been calculated.

discussed in terms of a blowout bifurcation. Increasing β further, we observe first a transition from SNA to an asynchronous chaotic attractor of same type as shown in Fig. 9(c) and 9(d) and second a transition from the small two-piece chaotic attractor to a big one-piece attractor similar to the interior crisislike transition in Fig. 9(e) and 9(f). The latter one grows for increasing β and disappears finally in a boundary crisis.

In Sec. III we have found chaotic as well as strange nonchaotic motion as synchronized regimes. The corresponding transitions to asynchronous motion are sketched in Fig. 4 by paths VI and VII. Path VI starts from synchronized chaotic motion and leads to an asynchronous chaotic attractor due to the usual blowout bifurcation (Fig. 11). This type of transition from synchronized to nonsynchronized chaotic attractor has been widely investigated [22].

Path VII in Fig. 4 represents again a different type of blowout transition, namely, from synchronized SNA to asyn-

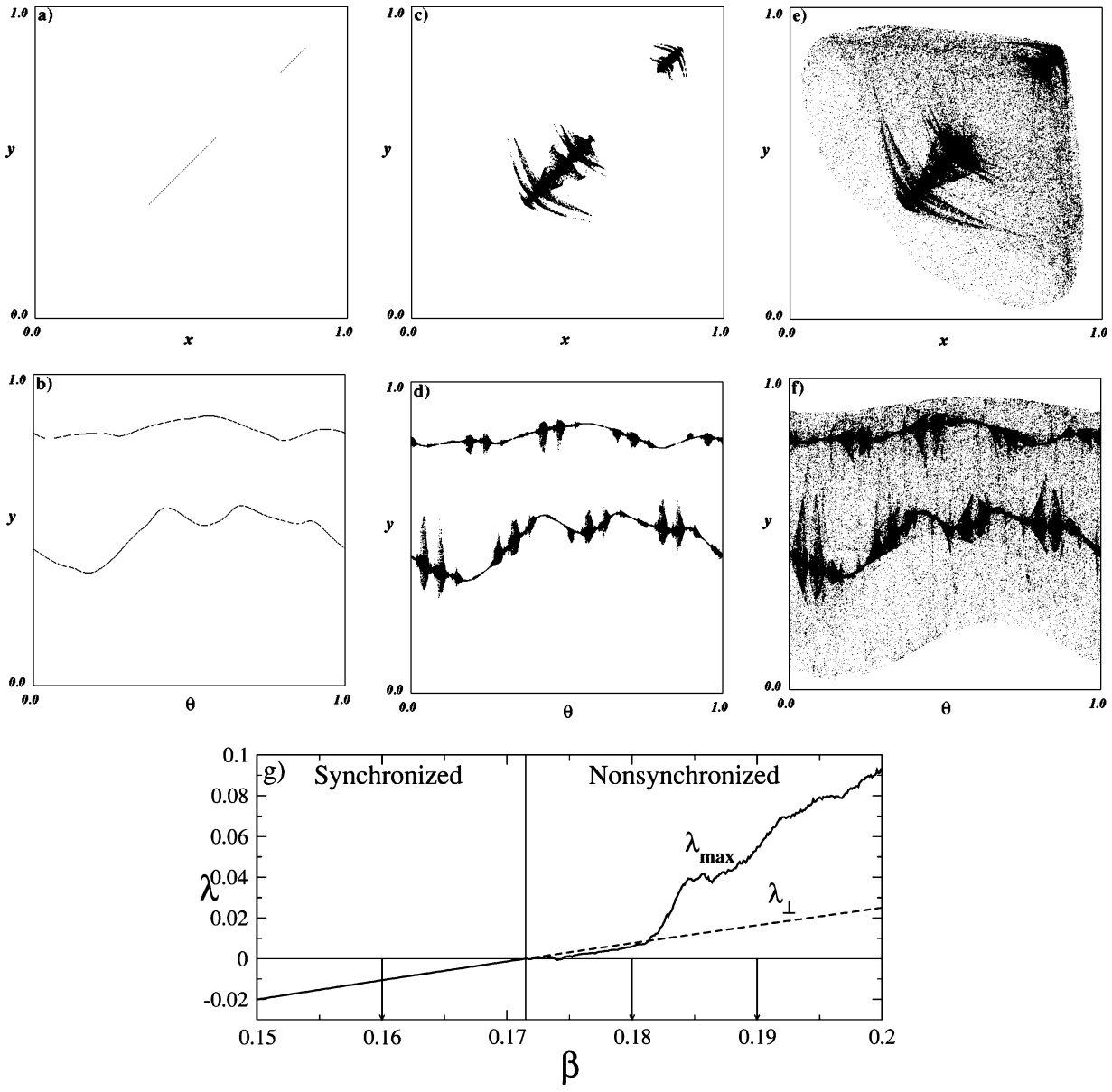

FIG. 9. Blowout transition from two synchronized invariant curves to a nonsynchronized chaotic attractor at $\epsilon=0.03, \alpha=3.35$ represented by path V in Fig. 4. Panels (a) and (b) show the synchronized attractor consisting of two invariant curves at $\beta=0.16$ as projection onto the (x,y) plane and onto the y-θ plane, respectively. Panels (c) and (d) show a nonsynchronized chaotic attractor at $\beta=0.18$ as a projection onto the x-y plane and onto the y-θ plane after the blowout transition. Panels (e) and (f) show a nonsynchronized chaotic attractor at $\beta=0.19$ as a projection onto the x-y plane and onto the y-θ plane after a sudden increase in size. Panel (g) shows the dependence of Lyapunov exponents $\lambda_\perp$ (dashed) and λ_{max} (solid) on the bifurcation parameter. The arrows mark the values of the bifurcation parameter β for which the attractors have been calculated.

chronous chaotic motion (Fig. 12). Before the bifurcation, at $\alpha=3.51$ the maximal Lyapunov exponent coinciding with the larger one of $\lambda_\perp$ and $\lambda_\parallel$ is negative as well as the transverse Lyapunov exponent. Thus, the synchronized dynamical regime is an SNA. The transverse Lyapunov exponent becomes positive at $\alpha\approx3.519$, i.e., a blowout bifurcation takes place. After the blowout bifurcation the maximal Lyapunov exponent is positive, too. Therefore, the nonsynchronized attractor is chaotic.

VI. CHARACTERISTICS OF THE DIFFERENT TYPES OF BLOWOUT TRANSITIONS

In Sec. V we have presented different types of blowout transitions from synchronized motion to nonsynchronous one. Two of those transitions we would like to characterize and to compare in more detail. We focus here on transitions from synchronized quasiperiodic motion on invariant curves to asynchronous chaotic behavior. Their difference becomes obvious from the different structure of the asynchronous at-

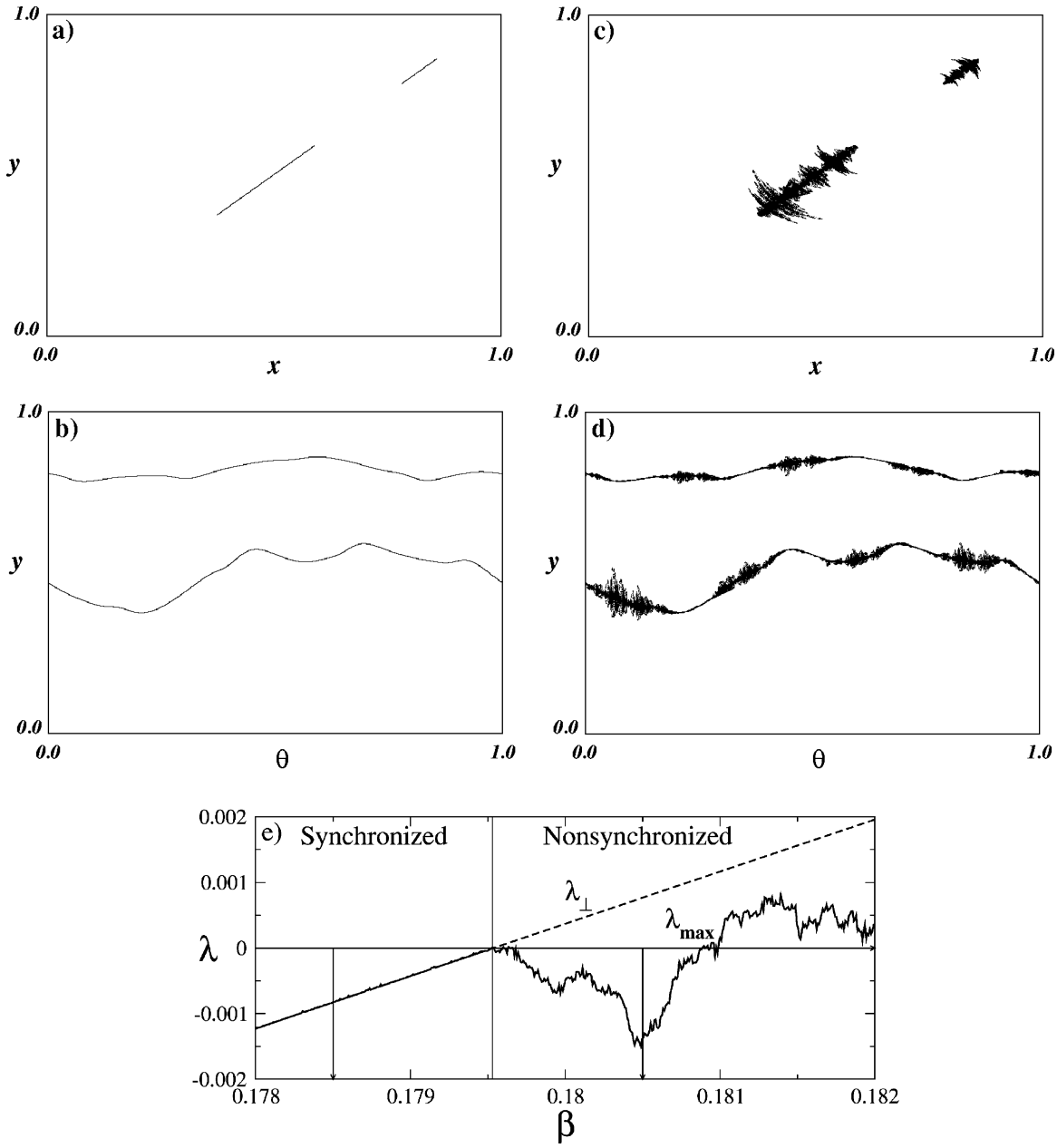

FIG. 10. Blowout transition from two synchronized invariant curves to nonsynchronized SNA at $\epsilon=0.03, \alpha=3.318$ represented by path V in Fig. 4. Panels (a) and (b) show the synchronized attractor consisting of two invariant curves at $\beta=0.1785$ as projection onto the (x,y) plane and onto the y-θ plane, respectively. Panels (c) and (d) show the nonsynchronized SNA at $\beta=0.1805$ as a projection onto the x-y plane and onto the y-θ plane after the blowout transition. Panel (e) shows the dependence of Lyapunov exponents $\lambda_\perp$ (dashed) and λ_{max} (solid) on the bifurcation parameter. The arrows mark the values of the bifurcation parameter β for which the attractors have been calculated.

tractor shortly after the blowout bifurcation [compare Figs. 8(c), 8(d), and Figs. 9(c), 9(d) and, similarly Figs. 10(c), 10(d)]. To compare the two transitions we use two different measures. Let us first discuss the growth of the attractor in size. To measure quantitatively the size of the attractor beyond the blowout bifurcation, we compute the mean value of the squared distance of points $\langle (x-y)^2 \rangle$ in the blown out attractor from the synchronization manifold, the diagonal D. For $\alpha=3.22$ beyond the critical value of β, a sudden strong growth of the attractor with increasing β is observed [Fig. 13(a)]. The same qualitative dependence on β has been obtained for the maximal Lyapunov exponent λ_{max} as well [Fig. 8(e)].

The other type of blowout bifurcation observed at $\alpha=3.318$ and $\alpha=3.35$ consists of two different phenomena. First, one observes a small, slowly growing asynchronous attractor with varying β. At some critical value of β, the asynchronous attractor starts to grow rapidly. These two subsequent bifurcations are illustrated in Fig. 13(b) for $\alpha=3.318$, where the width of the asynchronous attractor is shown in dependence on the bifurcation parameter β. The blowout transition happens at $\beta \approx 0.1795$ and the interior cri-

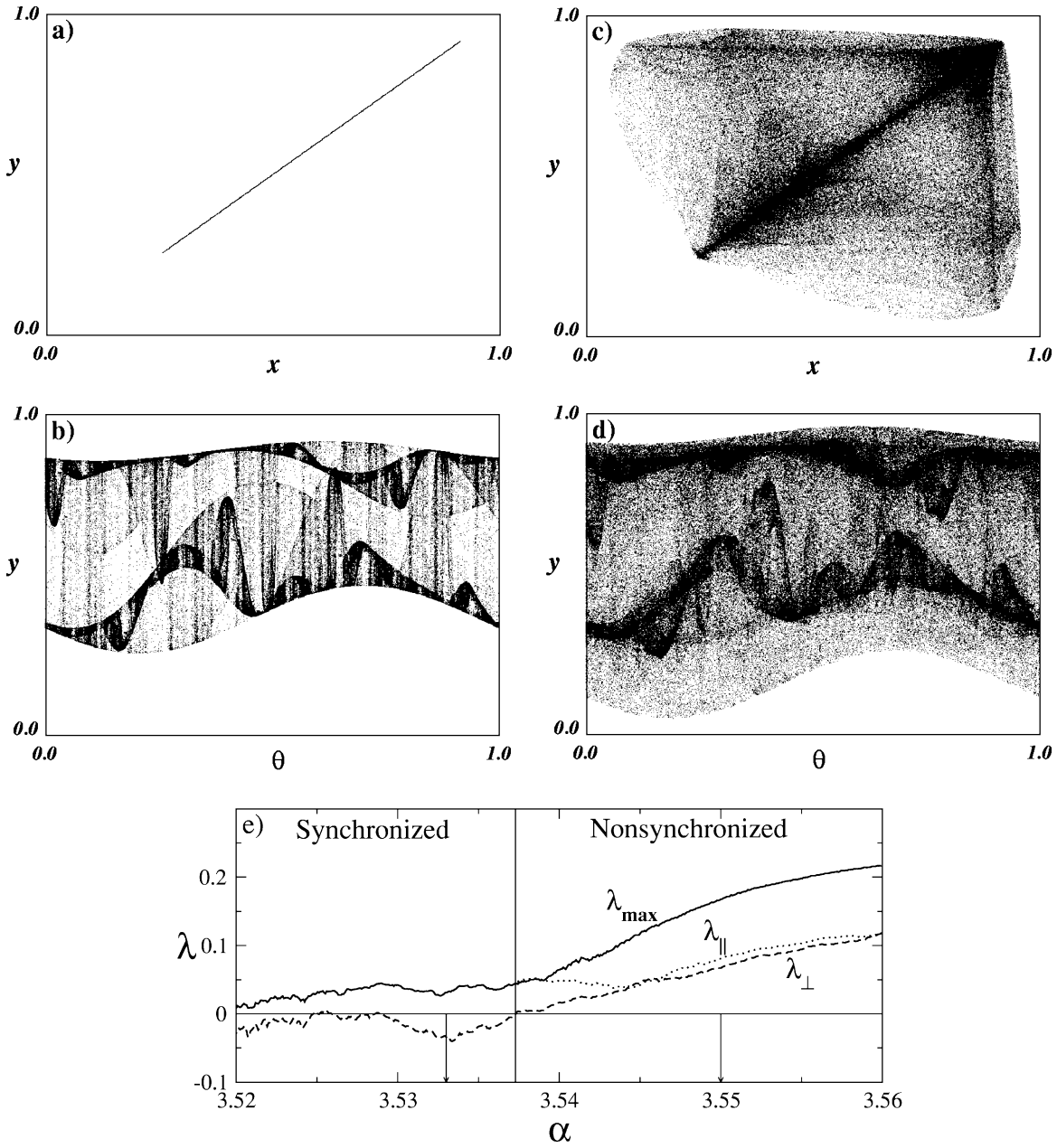

FIG. 11. Blowout transition from synchronized chaotic attractor to nonsynchronized chaotic attractor at $\epsilon=0.03, \beta=0.1$ represented by path VI in Fig. 4. Panels (a) and (b) show the synchronized chaotic attractor at $\alpha=3.533$ as projection onto the (x,y)-plane and onto the y-θ plane, respectively. Panels (c) and (d) show the nonsynchronized chaotic attractor at $\alpha=3.55$ as a projection onto the x-y plane and onto the y-θ plane after the blowout transition. Panel (e) shows the dependence of Lyapunov exponents $\lambda_\perp$ (dashed), $\lambda_\parallel$ (dotted), and $\lambda_{\max}$ (solid) on the bifurcation parameter. The arrows indicate the values of the bifurcation parameter α, for which the attractors have been calculated.

sislike transition characterized by a change in the speed of the growth of the attractor size occurs at $\beta \approx 0.1923$. Thus we call this transition only interior crisislike, since in contrast to the well studied interior crisis [23], we do not obtain a sudden growth in the size itself but, only in the growth rate of the size. Again the attractor width behaves like the Lyapunov exponent if the parameter β is varied beyond the critical value of the blowout bifurcation. For both transitions we obtain a scaling for the growth rate of the asynchronous attractor beyond the blowout bifurcation. For the blowout bifurcation from synchronized quasiperiodicity to asynchronous chaos we obtain a scaling according to a power law

$$\langle (x-y)^2 \rangle \sim (\beta-\beta_c)^\gamma, \tag{5}$$

where β_c denotes the critical value of β, where the blowout occurs. For $\alpha=3.22$ we computed $\gamma=0.15$ from a fit of a straight line to the data in double-logarithmic representation [Fig. 14(a)]. For $\alpha=3.318$ a similar scaling for the blowout bifurcation has been found, thus we focus on the second transition. For the interior crisislike transition the scaling of the mean size of the asynchronous attractor is linear. The

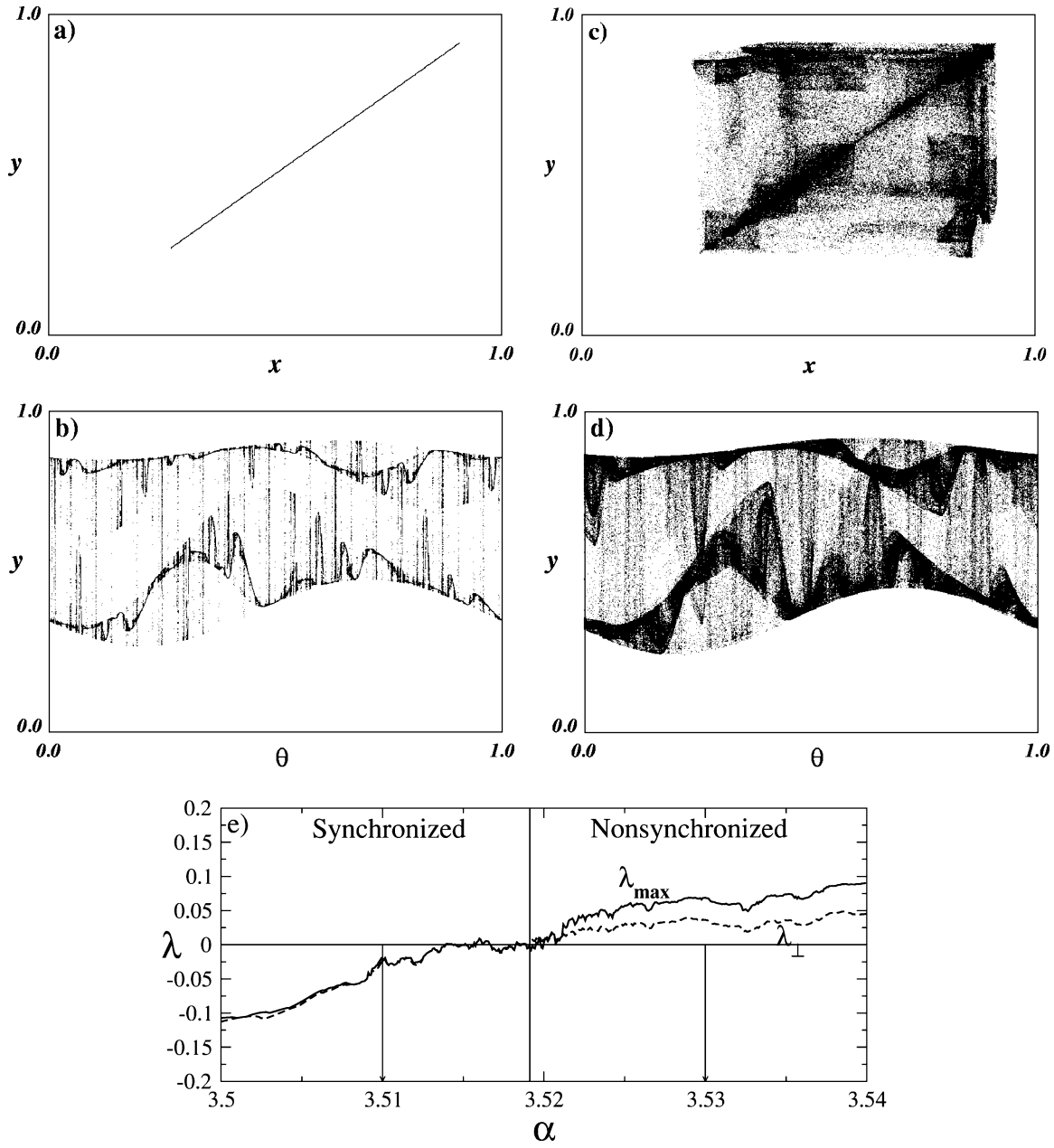

FIG. 12. Blowout transition from synchronized SNA to nonsynchronized chaotic attractor at $\epsilon=0.03, \beta=0.01$ represented by path VII in Fig. 4. Panels (a) and (b) show the synchronized SNA at $\alpha=3.51$ as a projection onto the (x,y) plane and onto the y-θ plane, respectively. Panels (c) and (d) show the nonsynchronized chaotic attractor at $\alpha=3.53$ as a projection onto the x-y plane and onto the y-θ plane after the blowout transition. Panel (e) shows the dependence of Lyapunov exponents $\lambda_\perp$ (dashed) and $\lambda_{\max}$ (solid) on the bifurcation parameter. The arrows indicate the values of the bifurcation parameter α, for which the attractors have been calculated.

different growth rates correspond to different slopes [Fig. 14(b)]. The characteristic slopes for this transition at $\alpha=3.318$ are 0.05 and 3.3.

Another approach to characterize the blowout transitions is to consider the intermittent behavior after the synchronized attractor became transversally unstable [23]. Figure 15(a) represents the time series $|x_n-y_n|$ in dependence on the iteration number n. Laminar phases correspond to the synchronized state, whereas bursts correspond to nonsynchronous states. By defining a threshold, we are able to determine the length τ of the laminar phases between two successive bursts larger than the threshold. So, we can compute the average time the trajectory spends close to the synchronization manifold. Figure 15(b) represents the average length $\langle\tau\rangle$ of laminar phases in dependence on the parameter mismatch $\beta-\beta_c$. In the log-log plot these data fit to a straight line, justifying again a power law dependence

$$\langle\tau\rangle\sim(\beta-\beta_c)^{-\gamma}, \tag{6}$$

with the critical exponent $\gamma=0.452$ at $\alpha=3.22$.

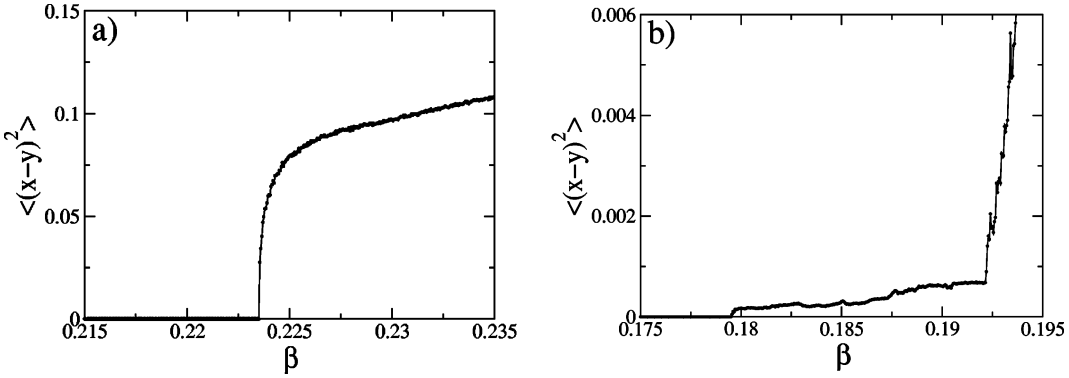

FIG. 13. Width of the asynchronous attractors in dependence on the bifurcation parameter β for (a) $\alpha=3.22$ and (b) $\alpha=3.318$.

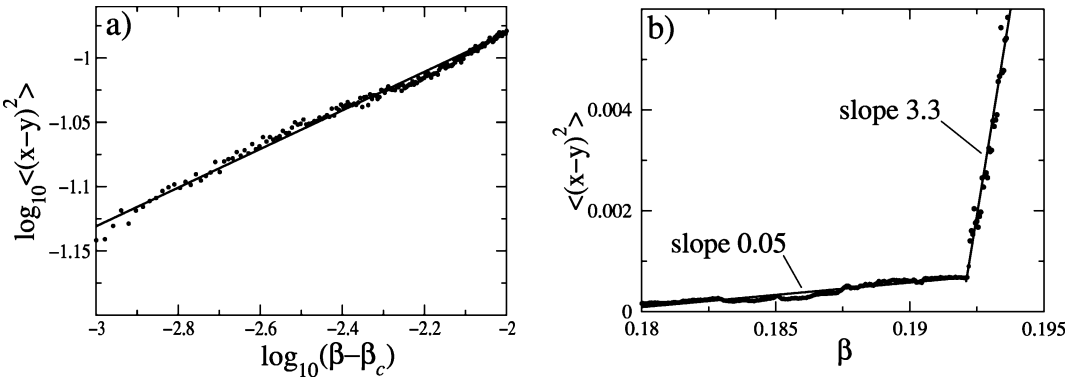

FIG. 14. Scaling behavior of the blowout transitions: (a) The width of the asynchronous attractor for $\alpha=3.22$ depends on the parameter mismatch $\beta-\beta_c$ according to a power law. (b) For $\alpha=3.318$ only the interior crisislike transition is shown. The small slope 0.05 characterizes the attractor growth rate of the small chaotic attractor, while the large slope 3.3 corresponds to the growth rate of the big attractor.

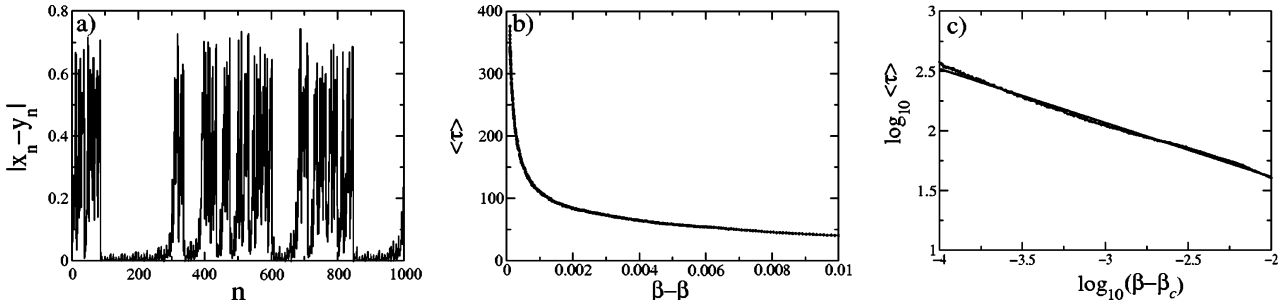

FIG. 15. Scaling of laminar phases for the blowout bifurcation at $\alpha=3.22$: (a) time series $\|x_n-y_n\|$, (b) distribution of mean time intervals of laminar phases, (c) scaling of the duration of laminar phases.

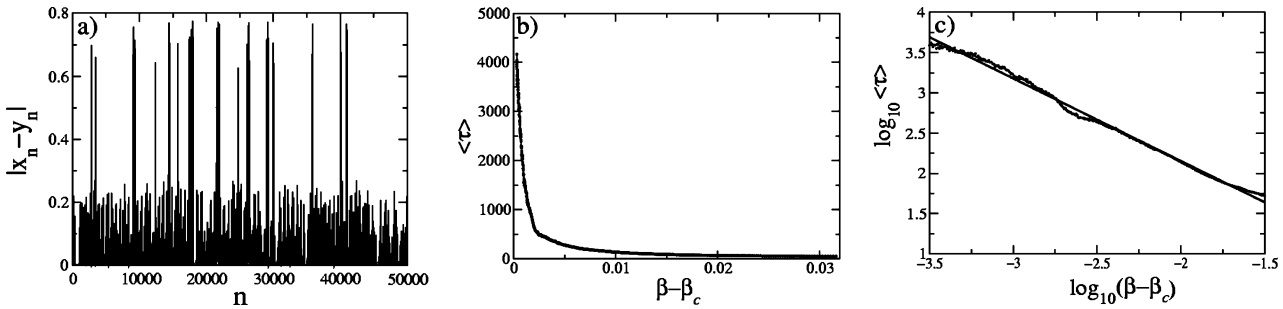

FIG. 16. Scaling of laminar phases for interior crisislike transition at $\alpha=3.318$: (a) time series $\|x_n-y_n\|$, (b) distribution of mean time intervals of laminar phases, (c) scaling of the duration of laminar phases.

For the interior crisislike transition at $\alpha=3.318$ and $\beta \approx 0.1923$ one can consider again the intermittent behavior. Now the laminar phases correspond to the situation that the trajectory spends time on the nonsynchronous chaotic attractor restricted to the narrow region near the synchronization manifold [Fig. 16(a)]. The average time of laminar phases depends on the parameter mismatch again via a power law [Eq. (5)], with the characteristic exponent $\gamma=1.03$ at $\alpha=3.318$ [Figs. 16(b), 16(c)].

VII. CONCLUSIONS

We have studied the influence of quasiperiodic driving on synchronization phenomena as well as on desynchronization. To this end, we have considered a system of two coupled quasiperiodically forced logistic maps. The dynamics in the synchronization region can be described by a single quasiperiodically forced logistic map. Therefore, the effects of the quasiperiodic driving on the synchronous motion are the same as known for the single system [16]: periodic orbits are transformed into invariant curves, hence the period-doubling cascade is converted into a doubling cascade of invariant curves, where the doublings are delayed as the forcing amplitude increases. Furthermore, the doubling cascade is truncated, i.e., branches of the treelike structured synchronization region are cutoff, first those corresponding to invariant curves of higher periodicities. Thus, with increasing forcing amplitude the synchronization region becomes smaller so that it becomes more and more difficult to obtain synchronized motion. For sufficiently high forcing amplitudes the synchronization is suppressed. Beside quasiperiodic motion on invariant curves, we find strange nonchaotic and chaotic behavior in the synchronization region. With respect to desynchronization, coexisting asynchronous attractors in the synchronization region play an important role for the type of transition to nonsynchronized motion. In case of their existence, the trajectory approaches the asynchronous attractor as the synchronized state loses the transverse stability. More interesting is the case if no asynchronous attractors coexist with synchronized ones. Then the loss of transverse stability of the synchronous attractor leads to the emergence of a new asynchronous attractor as a result of a blowout bifurcation. We have analyzed the possible types of blowout transition from different synchronized dynamical regimes to desynchronized atttractors. Beside the usual blowout from synchronized to nonsynchronized chaotic motion we have described two types of blowout transitions in detail. One of them is the blowout from synchronized quasiperiodic motion to a nonsynchronized chaotic attractor. The other corresponds to a transition from synchronized SNA to a nonsynchronized chaotic attractor. Both transitions can be identified by a change in sign of the transverse Lyapunov exponent only. Other characteristics known from usual blowout bifurcations, such as the loss of transverse stability of embedded unstable periodic orbits cannot be used because of the lack of such orbits. Additionally, we found an interior crisislike transition in which the growth rate of the blown out attractor changes discontinously. The exact mechanism of this transition is not fully understood and needs some further investigation which is under way. Furthermore, we have identified a vertex point in parameter space, where four different bifurcation lines meet. On one hand the transverse instability of the synchronous attractor in the diagonal becomes a blowout bifurcation. On the other hand the merging crisis of the asynchronous attractor meets the boundary crisis of the asynchronous attractor. At the vertex point itself the synchronous as well as the asynchronous attractor are involved in the bifurcation.

Finally we would like to remark that all bifurcations described in this paper can also occur in invertible maps and thus also in flows, where quasiperiodic motion occours on invariant tori. Noninvertibility is not the reason for any of the bifurcations analyzed in this paper. It has been used only to keep the analysis as simple as possible.

ACKNOWLEDGMENTS

We would like to thank P. Ashwin, E. Ott, O. Popovych, and S. Popovych for valuable discussions. Furthermore we thank the Deutsche Forschungsgemeinschaft (Grant No. Sfb 555) for financial support.

[1] M.G. Rosenblum, A.S. Pikovsky, and J. Kurths, Phys. Rev. Lett. **76**, 1804 (1996).
[2] L.M. Pecora and T.L. Carroll, Phys. Rev. Lett. **64**, 821 (1990).
[3] N.F. Rulkov, M.M. Sushchik, L.S. Tsimring, and H.D.I. Abarbanel, Phys. Rev. E **51**, 980 (1995).
[4] L. Kocarev and U. Parlitz, Phys. Rev. Lett. **76**, 1816 (1996).
[5] Y.-C. Lai, C. Grebogi, J.A. Yorke, and S.C. Venkataramani, Phys. Rev. Lett. **77**, 55 (1996).
[6] E. Ott and J.C. Sommerer, Phys. Lett. A **188**, 39 (1994).
[7] P. Ashwin, J. Buesco, and I. Stewart, Nonlinearity **9**, 703 (1996).
[8] R. Ramaswamy, Phys. Rev. E **56**, 7294 (1997).
[9] Yu.L. Maistrenko, V.L. Maistrenko, A. Popovich, and E. Mosekilde, Phys. Rev. E **57**, 2713 (1998).
[10] Yu.L. Maistrenko, V.L. Maistrenko, O. Popovych, and E. Mosekilde, Phys. Rev. E **60**, 2817 (1999).
[11] E. Mosekilde, Yu. Maistrenko, and D. Postnov, *Chaotic Synchronization, Applications to Living Systems*, edited by Leon O. Chua, World Scientific Series on Nonlinear Science, Series A Vol. 42 (World Scientific, Singapore, 2002).
[12] S. Yousefi, Yu. Maistrenko, and S. Popovych, Discrete Dyn. Nat. Soc. **5**, 161 (2000).
[13] C. Grebogi, E. Ott, S. Pelikan, and J.A. Yorke, Physica D **13**, 261 (1984).
[14] A.S. Pikovsky and U. Feudel, Chaos **5**, 253 (1995).
[15] T.E. Vadivasova, O.V. Sosn ovtseva, A.G. Balanov, and V.V. Astakhov, Phys. Rev. E **61**, 4618 (2000).
[16] J.F. Heagy and S.M. Hammel, Physica D **70**, 140 (1994).
[17] S. Kuznetsov, U. Feudel, and A. Pikovsky, Phys. Rev. E **57**, 1585 (1998).

[18] J. Milnor, Commun. Math. Phys. **99**, 177 (1985).
[19] T. Nishikawa and K. Kaneko, Phys. Rev. E **54**, 6114 (1996).
[20] A. Prasad, V. Mehra, and R. Ramaswamy, Phys. Rev. Lett. **79**, 4127 (1997).
[21] T. Yalcinkaya and Y.-C. Lai, Phys. Rev. Lett. **77**, 5039 (1996).
[22] A.S. Pikovsky and P. Grassberger, J. Phys. A **24**, 4587 (1991); J.C. Sommerer and E. Ott, Nature (London) **365**, 136 (1993); E. Ott and J.C. Sommerer, Phys. Lett. A **188**, 39 (1994).
[23] C. Grebogi, E. Ott, and J.A. Yorke, Phys. Rev. Lett. **48**, 1507 (1982); C. Grebogi, E. Ott, and J.A. Yorke, Physica D **7**, 181 (1983); C. Grebogi, E. Ott, F. Romeiras, and J.A. Yorke, Phys. Rev. A **36**, 5365 (1987).